ACS APPLIED MATERIALS & INTERFACES

www.acsami.org

Research Article

Methodology to Detect Biological Particles Using a Biosensing Surface Integrated in Resistive Pulse Sensing

Yukichi Horiguchi,* Norihiko Naono, Osamu Sakamoto, Hiroaki Takeuchi, Shoji Yamaoka, and Yuji Miyahara

Cite This: *ACS Appl. Mater. Interfaces* 2022, 14, 20168–20178

Read Online

ACCESS | Metrics & More | Article Recommendations | Supporting Information

ABSTRACT: Resistive pulse sensing (RPS) is an analytical method that can be used to individually count particles from a small sample. RPS simply monitors the physical characteristics of particles, such as size, shape, and charge density, and the integration of RPS with biosensing is an attractive theme to detect biological particles such as virus and bacteria. In this report, a methodology of biosensing on RPS was investigated. Polydopamine (PD), an adhesive component of mussels, was used as the base material to create a sensing surface. PD adheres to most materials, such as noble metals, metal oxides, semiconductors, and polymers; as a result, PD is a versatile intermediate layer for the fabrication of a biosensing surface. As an example of a biological particle, human influenza A virus (H1N1 subtype) was used to monitor translocation of particles through the pore membrane. When virus-specific ligands (6′-sialyllactose) were immobilized on the pore surface, the translocation time of the virus particles was considerably extended. The detailed translocation data suggest that the viral particles were trapped on the sensing surface by specific interactions. In addition, virus translocation processes on different pore surfaces were distinguished using machine learning. The result shows that the simple and versatile PD-based biosensor surface design was effective. This advanced RPS measurement system could be a promising analytical technique.

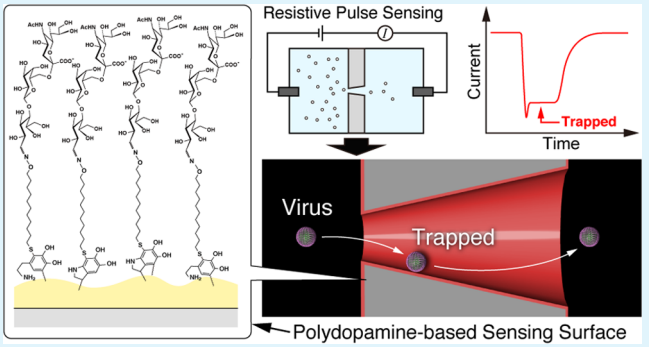

KEYWORDS: *resistive pulse sensing, biosensor, polydopamine, virus, machine learning*

INTRODUCTION

Resistive pulse sensing (RPS) is a candidate for early diagnosis. RPS, also known as the Coulter principle,[1] can detect particle translocation through a pore membrane by monitoring the ionic current flow. This technique can obtain information on the number of particles and their size, which are useful for the measurement of biological molecules or particles.[2] Therefore, artificial pores for RPS measurement have been developed for the detection of nucleic acids,[3,4] peptides,[5] proteins,[6−9] viruses,[10−14] bacteria,[15,16] and extracellular vesicles.[17−20] An advantage of RPS is that the particles can be analyzed individually, which allows for monitoring the physical characteristics of the analytes such as size, shape, and charge density.[21−26] Dynamic light scattering, particle tracking analysis, differential centrifugal sedimentation, and transmission electron microscopy (TEM) are conventional particle measurement techniques. RPS can be used to calculate the particle size distribution using an individual particle analysis similar to techniques such as TEM.[21] However, RPS cannot usually monitor the biological information of the particles. For example, particle analytical methods, such as microcapillary electrophoresis with a laser dark-field microscope[19] and asymmetric flow field-flow fractionation,[20] can be used to evaluate the characteristics of biological particles. Therefore, integration of biosensing on RPS is an attractive theme to expand the scope of the RPS application.

Typical detection methods for biomolecules, such as western blotting and enzyme linked immunosorbent assays, use specific interactions for target detection. The core technology for specific detection is the design of a biosensing surface, which affects the detection performance. For example, the sensing performance of a label-free biosensing system, such as surface plasmon resonance (SPR), quartz crystal microbalance (QCM), and surface acoustic wave (SAW)-based biosensor, strongly depends on the biosensing surface fabricated on a gold sensor chip.[27,28] Therefore, a methodology for a biosensing surface integrated with RPS may be an advanced analytical technique.

Received: December 27, 2021
Accepted: April 11, 2022
Published: April 21, 2022

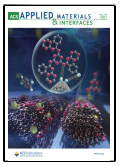

https://doi.org/10.1021/acsami.1c25006
ACS Appl. Mater. Interfaces 2022, 14, 20168−20178

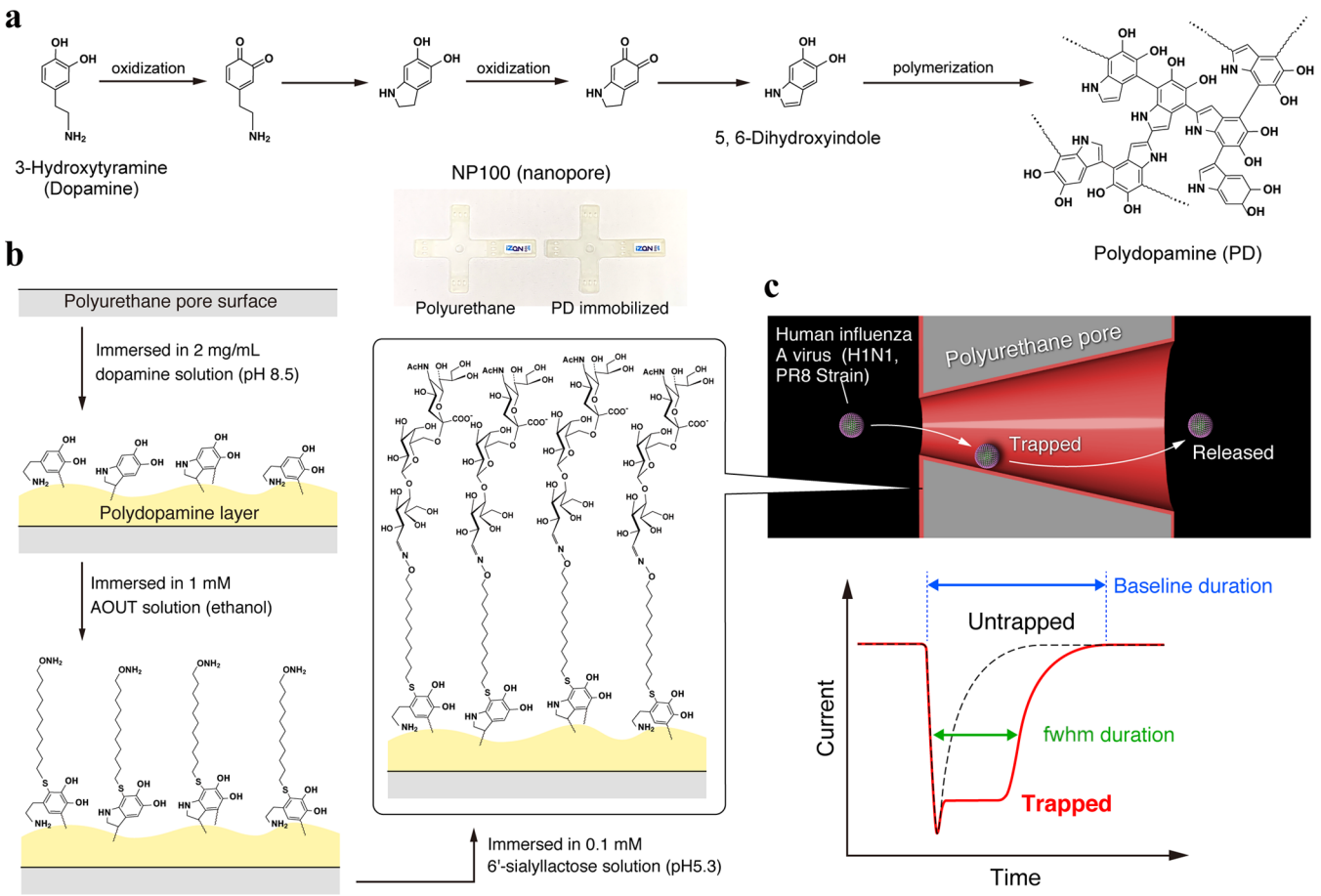

Figure 1. Conceptual rendering of this work. (a) Polymerization scheme of PD. 3-Hydroxylthyramine (dopamine) becomes 5,6-dihydroxyindole through oxidization. The PD layer is formed by oxidation polymerization from 5,6-dihydroxyindole. (b) Strategy of surface modification on the pore surface. The polyurethane nanopore was immersed in a dopamine solution to form a PD layer on the surface. PD is a melanin-like structure on the pore that was clearly stained dark. AOUT was immobilized on the PD layer via Michael-type addition. 6′-siallylactose was immobilized on an aminooxy-moiety on the surface via glycoblotting. (c) Illustration of the viral particle measurement. If a particle is trapped on the biosensing surface, differences in the translocation process cause differences in the waveform compared with the untrapped case.

A common method to monitor specific interactions using RPS is the conjugation technique. For example, antigen and antibody interactions form conjugates, which produce a size change in the analytes.[10,29] It is also possible to prepare particles immobilized with ligands that bind specifically to the analyte and then confirm the presence of the analyte by aggregation or complex formation.[7,30,31] Nanocarrier-based detection systems have also been reported. In this technique, sensing ligands, such as nucleic acid and peptides, are immobilized on the nanoparticles (nanocarriers); the surface characteristic changes on the nanocarriers derived from the detection of analytes were evaluated using RPS measurements.[32,33] The other approach is immobilization of ligands on a pore surface.[9,34−36] This technique generates biological interactions between the pore surface and analytes, which are recorded as changing the ion current or the translocation time.[36−38]

Functionalization of pore surfaces has been emphasized along with the development of RPS, and various functions, such as rectification, can be introduced to the pores.[39−44] The materials of the pores used for functionalization are also diverse, including semiconductors,[12] glass,[40] and various kinds of polymer membranes.[41,45−47]

Based on the above reasons, an investigation of pore functionalization can enhance the value of RPS.[43,44] One problem is the fabrication process of a biosensing surface on a pore because the surface modification is restricted by the base material of the pore surface. In previous reports, pores were prepared in a variety of materials, such as quartz, semiconductors, and polymers, making it difficult to simplify the surface modification process. Development of a versatile fabrication methodology to create a biosensing surface on a pore surface could make the RPS measurement an advanced biosensing system.

A polydopamine (PD) layer-based biosensing surface is a promising candidate to fabricate the biosensing surface on a pore surface. PD is an adhesive component of mussels, and it can adhere to most materials such as noble metals, metal oxides, semiconductors, and polymers.[48] In addition, PD can be further immobilized using amine- or thiol-terminated molecules via a Schiff-base reaction or Michael-type addition.[49] Therefore, PD may be a versatile intermediate layer for the fabrication of a biosensing surface. The validity of this functionalization method on extremely small pore surfaces for RPS was confirmed in our previous reports.[50,51]

In this report, the fabrication of a PD-based biosensing surface on a pore for RPS was investigated. The experiments were performed using qNano, a platform for tunable resistive pulse sensing (TRPS). TRPS can control the pore size by tensile force (called stretch) to optimize the measurement

https://doi.org/10.1021/acsami.1c25006
ACS Appl. Mater. Interfaces 2022, 14, 20168−20178

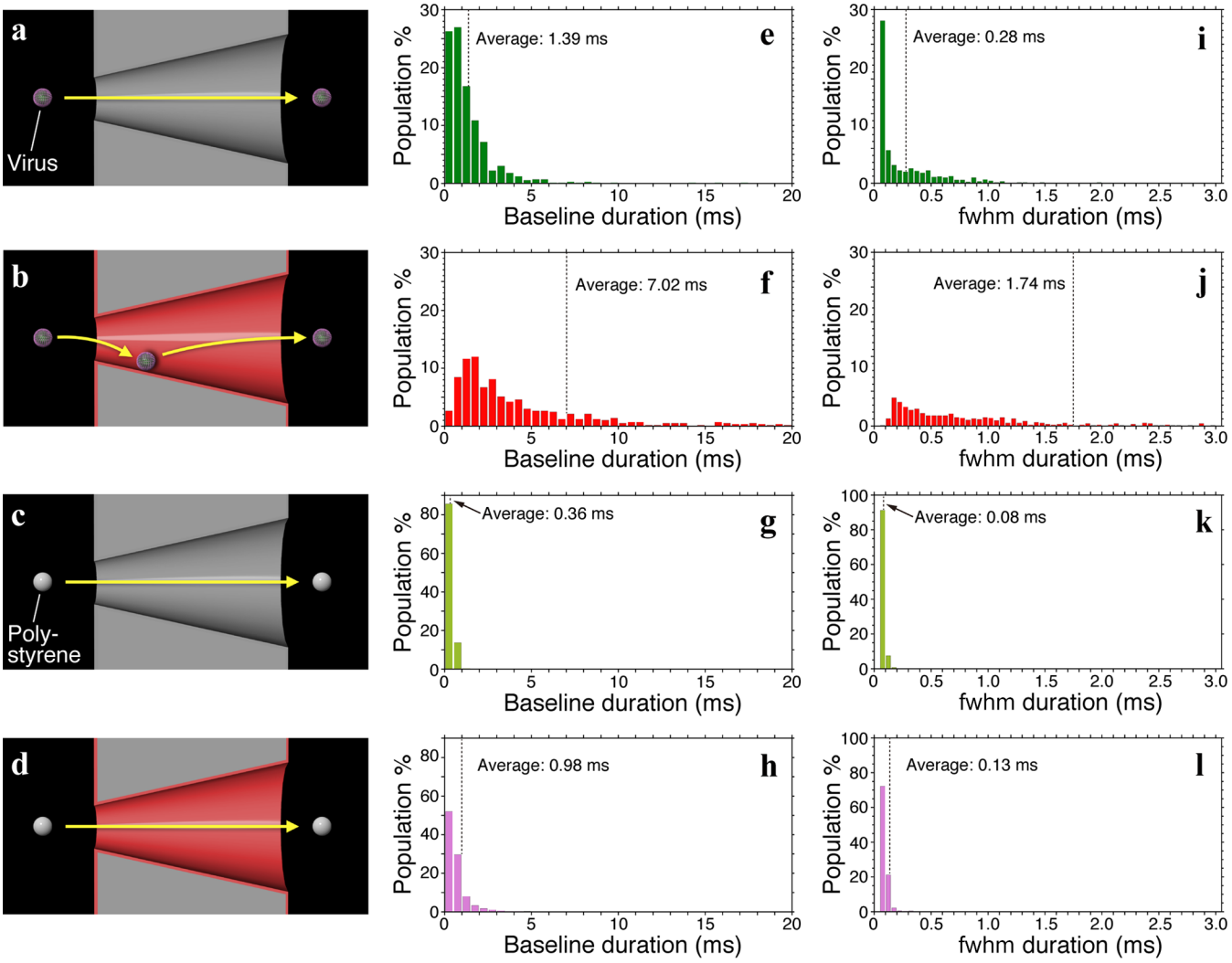

Figure 2. Illustration of the RPS measurements and histograms of the duration of ion current pulses. Viral particles were measured using a (a) bare polyurethane and (b) 6′-siallylactose-immobilized pore. As a control, polystyrene particles were measured using the same surfaces (c,d). (e–h) Baseline and (i–l) fwhm duration histogram of each experimental result.

condition for the target particle size,[52] which is suitable for biological particles such as viral particles and bacteria that are approximately a hundred nanometers to several micrometers in size.[53,54] Human influenza A virus (H1N1, PR8 strain) was used as a model of biological nanoparticle. The influenza virus is an envelope virus with a diameter of 80–120 nm,[55] and it has hemagglutinin spike protein that binds sialic acid expressed on a cell surface for infection.[56] For example, human influenza virus recognizes the Neu5Acα(2–6)Gal moiety on a cell surface. Therefore, 6′-sialyllactose (Neu5Acα(2–6)Galβ(1–4)Glc) was immobilized on the pore surface for biosensing. Recently, machine learning for RPS has emerged as a technology for analytical systems.[12–14,16] Interestingly, this technique uses the information of a waveform (measured pulse shape) to distinguish analyte types. Machine learning is accurate enough to identify subtypes of influenza viruses that are nearly identical in characteristics.[13] Therefore, translocation processes of virus particles on a PD-based biosensing pore surface were also evaluated using machine learning.

RESULTS AND DISCUSSION

Immobilization Strategy of a Ligand on the Pore Surface and Virus Measurements. A conceptual rendering of this work is shown in Figure 1. The key PD layer material was immobilized on the pore surface by oxidation polymerization.[50,51] When dopamine is dissolved in Tris-buffer, it starts to oxidize immediately. Oxidized dopamine became 5,6-dihydroxyindole and then formed PD by oxidation polymerization (Figure 1a).

In this report, the RPS measurement was performed using "qNano Gold," a commercially available nanoparticle analyzing system. The pores for qNano are prepared by penetration of a polyurethane membrane using a needle;[52] therefore, the materials of the pores are completely polyurethane, and the shape of the pore is conical.[54] Most material types, including noble metals and polymers, can be coated by a PD layer when the materials were immersed in a dopamine solution.[34] After soaking in the dopamine solution, the polyurethane pore was stained dark color because PD is a melanin-like structure (Figure 1b). Therefore, the PD coat can be confirmed visually.

After immobilization of the PD layer, the pore was immersed in a 11-aminooxy-1-undecanethiol (AOUT) solution (etha-

https://doi.org/10.1021/acsami.1c25006
ACS Appl. Mater. Interfaces 2022, 14, 20168–20178

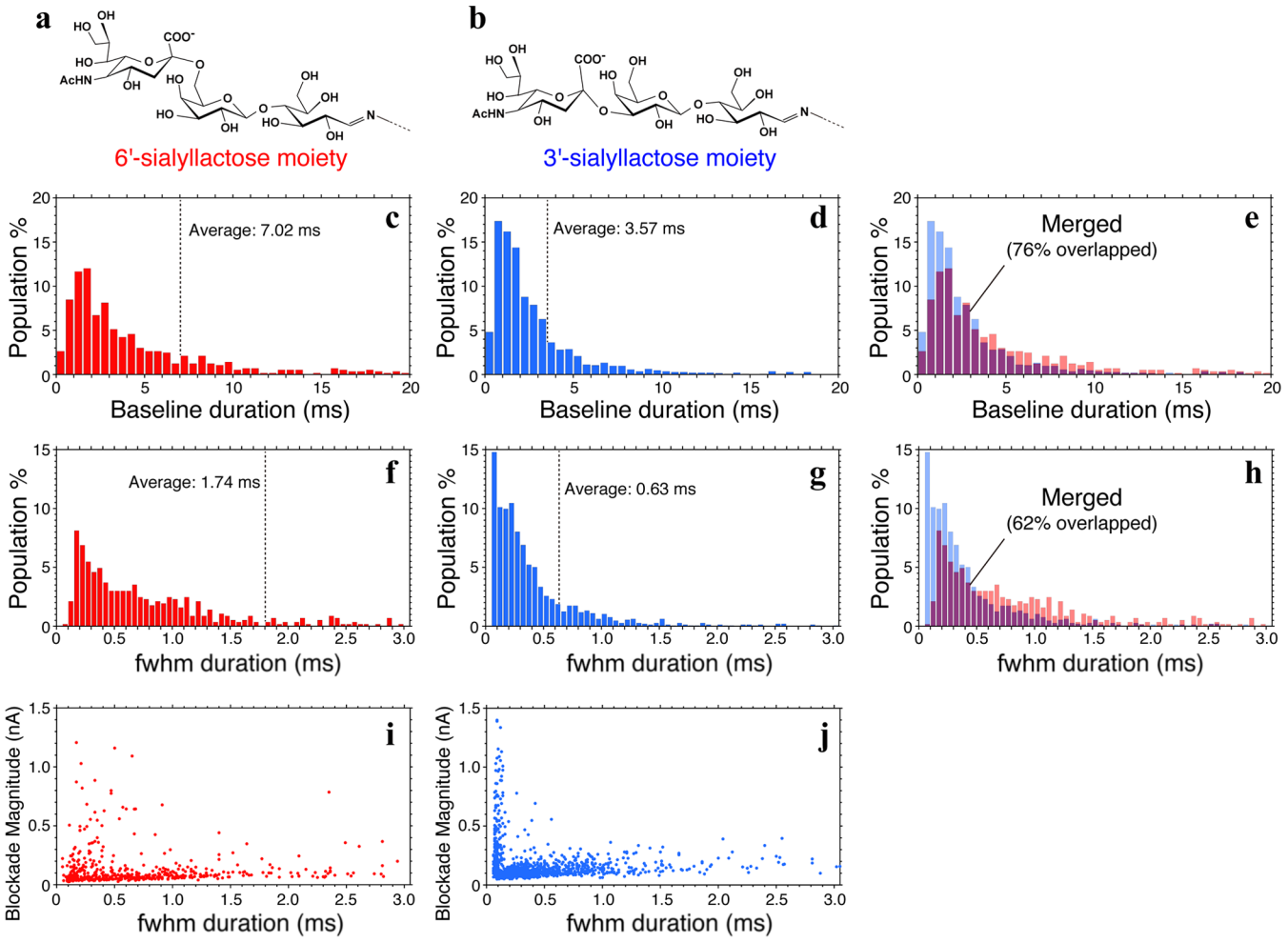

Figure 3. Result of the virus measurements using a (a) 6′-siallylactose (specific) and (b) 3′-siallylactose (nonspecific)-immobilized pore surface. (c–e) Baseline duration histograms of 6′-siallylactose (red), 3′-siallylactose (blue), and merged. (f–h) fwhm duration histograms of 6′-siallylactose (red), 3′-siallylactose (blue), and merged. 76 and 62% of the area overlapped on the baseline and fwhm duration histograms, respectively. (i,j) Scatter plots of individual measured pulse on 6′-siallylactose (n = 566) and 3′-siallylactose (n = 1433). The average baseline ion current values were 56.5 and 59.8 nA, respectively. (c,f) are the same data from Figure 2f,j used to compare the results.

nol). In this process, the thiol moiety of AOUT reacts with the PD layer via Michael-type addition.[49] The validity of this technique for pore immobilization was previously reported.[50,51] 6′-Sialyllactose was immobilized on an aminooxyl moiety via the glycoblotting technique.[57,58] To confirm 6′-sialyllactose immobilization on the PD layer, the same experiment was performed on a QCM sensor chip. After immobilization of the PD layer on the QCM sensor chip (4.21 ± 0.08 ng/mm^2, n = 3, Table S1), 6′-sialyllactose was immobilized on the PD layer. As a result, 2.15 ± 0.09 molecules/nm^2 (n = 3) of 6′-siallylactose were immobilized on the PD layer (Table S2). This result is not necessarily the same on PD layers formed on pore surfaces; however, it is useful for understanding the binding of 6′-sialyllactose to the PD layer.

The baseline ion current value was reduced from 82.4 ± 0.6 to 55.3 ± 3.1 nA (n = 3), which is due to the pore closure following the pore immobilization procedure. The size of the nanopore for qNano is not uniform because pores are prepared by penetration with a polycrystalline tungsten needle.[52] Pore geometries and current value characteristics have been previously described for measurements of 100 nm polystyrene nanoparticles.[59] In this study, the diameter of the narrowest part of the pore is approximately 1 μm in a stretched position, and the thickness of the pore is approximately 160–200 μm.[59,60] In addition, the resistance of the conical pore depends on the diameters of the narrowest and widest part.[59] Therefore, the change in pore diameter due to layer formation can be estimated from the change in ion current. Since the diameter of the widest part is several tens of micrometers, the effect of the current value change by layer formation is almost negligible, and the diameter change of the narrowest part affects the current value change predominantly. As a result, the ion current value is proportional to the diameter of the narrowest part almost linearly. In this immobilization procedure, approximately 30% of ion current was reduced after pore immobilization, which indicates that a biosensing film with a thickness of approximately 150 nm was formed on the pore surface. Although not a model for conical pores, another previous report has also shown that the ion current value is proportional to the pore diameter linearly.[61] Therefore, this estimation would be reasonable.

Human influenza A virus (H1N1, PR8 strain) was measured using this pore surface to evaluate the prepared biosensing surface on a pore (Figure 1c). When a particle traversed the pore membrane, the ion flow blocked by this translocation changes the ion current, which is called a pulse. If the viruses

https://doi.org/10.1021/acsami.1c25006
ACS Appl. Mater. Interfaces 2022, 14, 20168–20178

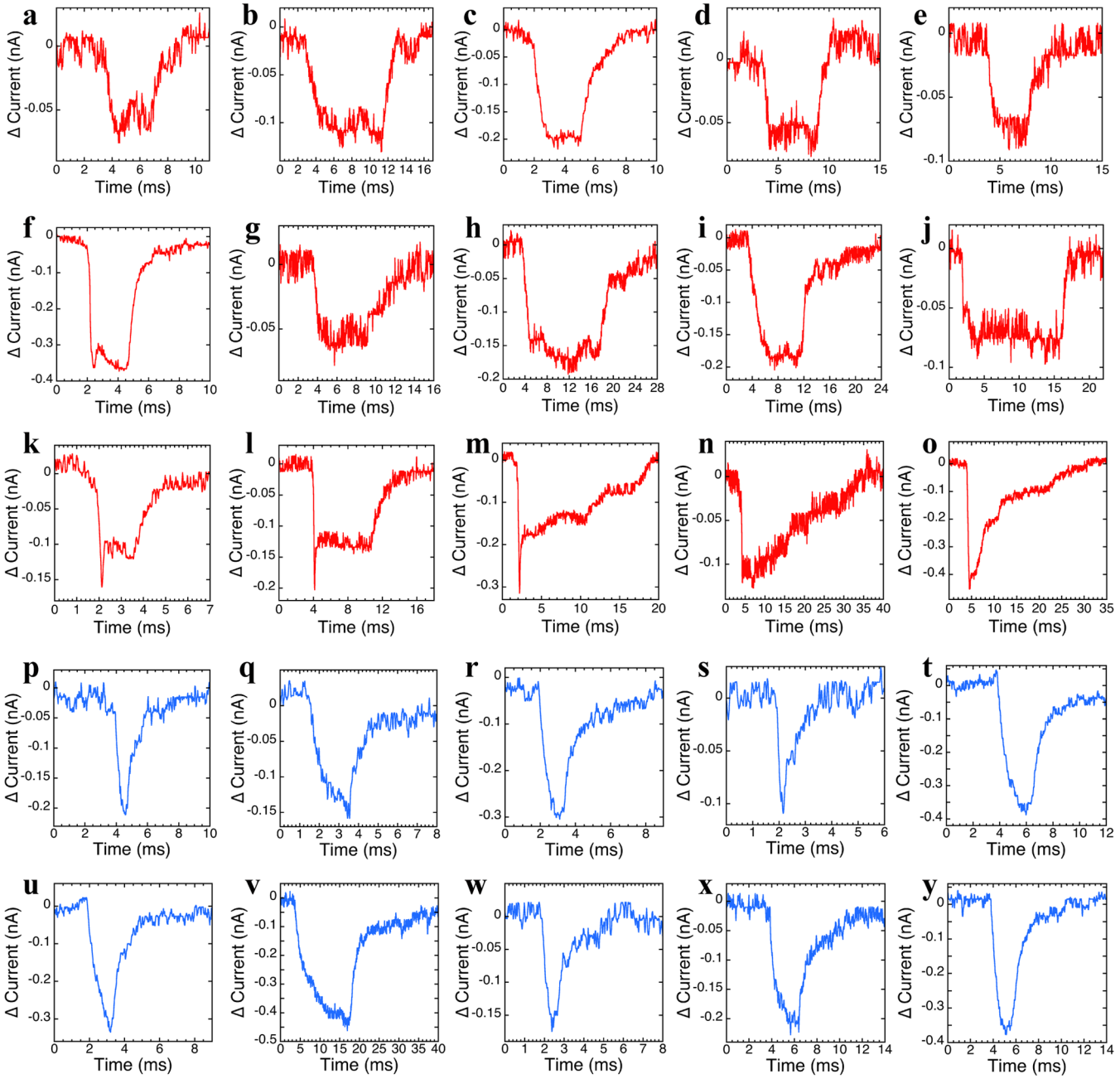

Figure 4. Extracted individual pulses measured on the (a−o) 6′-sialyllactose-immobilized pore (red) and (p−y) 3′-sialyllactose-immobilized pore (blue).

interacted with the biosensing surface, the virus particles were trapped during the translocation process, which extends the translocation time.

The results are shown in Figure 2. In this experiment, the virus particles were measured using an intact bare polyurethane pore (Figure 2a) and a 6′-siallylactose-immobilized pore (Figure 2b). As a control experiment, standard polystyrene nanoparticles (mode size: 110 nm, mean size: 110 nm) were also measured using the two pores (Figure 2c,d). The qNano particle measurement system provides two time parameters from the obtained pulses (Figure 1c). One is a baseline duration that represents the time until the current value returns to the baseline. The other is the full width at half-maximum (fwhm) duration, which is calculated by the pulse half-width relative to the pulse wave height. Both time parameters depend on the translocation of the particles; the fwhm duration is especially used as a translocation time of the particle through a pore.[26,62] The baseline duration and fwhm duration of each result are shown in Figure 2e−l.

According to this result, both the baseline and fwhm duration times of the virus measurement considerably increased when 6′-siallylactose ligands were immobilized on the pore surface. The average of the translocation time of the virus particles increased from 0.28 to 1.74 ms. The mode peak in Figure 2i completely disappeared in Figure 2j, which means that nearly all of the translocation processes of the virus particles were affected by the biosensing surface on the pore. The dissociation constant (K_d) between the influenza virus and sialic acid immobilized surface is 1×10^{-7} M;[63] therefore, virus particles trapped by this interaction increase the translocation

https://doi.org/10.1021/acsami.1c25006
ACS Appl. Mater. Interfaces 2022, 14, 20168−20178

time. Note that the fwhm duration time of some virus particles was greater than 3.0 ms (outside of the graph), indicating that several particles were trapped by the specific interaction. The complete dataset is shown in the Supporting Information as scatter plots (Figure S1).

As a control experiment, polystyrene standard nanoparticles were also applied to the same pore surfaces. The average translocation time was slightly increased (Figure 2k,l), though not remarkably, compared with the virus translocation time. There are some possible reasons for this result. The pore size is reduced because of the immobilization of the sensor surface, which creates a slight delay in passing the particles. The presence of electroosmotic flow could also be a reason for this delay. In the case of the 6′-siallylactose-immobilized surface, the surface charge becomes anionic in the neutral condition because the pK_a value of sialic acid is 2.6.[64] The generated electroosmotic flow by the counter cation layer opposes the pressure-driven flow and any electrophoresis for the particles and may cause a delay of translocation. Nonspecific weak interactions, such as van der Waals force and hydrogen bonds, are also potential reasons for this delay. In any case, strong trapping was not observed in the case of polystyrene particles.

Translocation Difference between Specific and Nonspecific Surfaces. The previous results confirm that the measured particles interacted with the biosensing surface, which increases the translocation time. Alternatively, the pore size decreased by the modification process, which may affect the translocation time. This reduction is derived from the pore closure by the modified sensing layer. To more clearly understand the specific interaction between the virus and the biosensing surface on a pore, 3′-siallylactose, a known receptor of the avian influenza virus, and a similar chemical structure to 6′-siallylactose (Figure 3a,b), was immobilized for nonspecific experiments. The average ion current value of the prepared 3′-siallylactose-immobilized pore was 55.0 ± 4.4 nA (n = 3), which is near the value of the 6′-siallylactose-immobilized pore. Both the baseline and fwhm durations of the 3′-siallylactose-immobilized surface (Figure 3d,g) were shorter than that of 6′-siallylactose (Figure 3c,f), which indicates that the specific interaction affected the translocation process of the virus particles. The average fwhm translocation time was nearly 3 times longer than the nonspecific interaction. To confirm the reproducibility, the same experiment was repeated three times using different pores, and similar results were observed (Figure S2). However, the distribution area of the translocation times for 6′-siallylactose and 3′-siallylactose widely overlapped (Figure 3e,h); therefore, whether a pulse is specific or nonspecific cannot be simply distinguished by the translocation time. The trapping of the viral particles on the biosensing surface is a stochastic phenomenon; some particles are trapped over a long time and some particles are trapped over a short time. Therefore, a more detailed evaluation of the extended translocation time because of the particle−surface interaction is needed.

The individual pulses obtained from the translocation of the viral particles were evaluated to understand the translocation process of each viral particle. Figure 4 shows the representative measured pulses using a pore immobilized with 6′-sialyllactose (specific, red) or 3′-sialyllactose (nonspecific, blue), which can demonstrate the interaction with the pore visually. The transition of the current stopped temporarily in the translocation process when the viruses were measured using the 6′-sialyllactose pore (Figure 4a−o). For example, the pulses in Figure 4a−j showed that current values had temporarily stopped at the bottom and then returned to the initial level. Accordingly, it is expected that viral particles were trapped by the 6′-sialyllactose surface. As mentioned in Figure 3, the translocation time was statistically longer on specific surfaces (6′-sialyllactose) than on the nonspecific surface (3′-sialyllactose). Alternatively, there are some cases where the translocation time of virus particles is long even though the surface is nonspecific (Figure 4p−y). The waveforms of these two groups are different.

The expected translocation processes of the viral particles are shown in Figure 5. A typical case is the transition of current

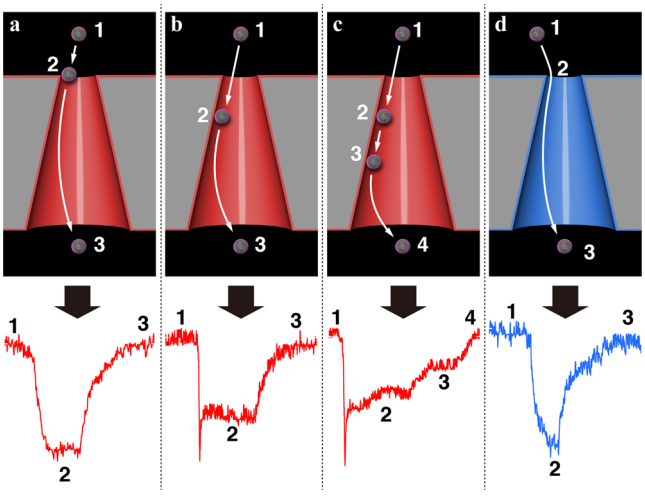

Figure 5. Expected translocation processes of a viral particle from the pulse shape. (a) Translocation type of Figure 4a−j. The virus particles were trapped at the narrowest point of the pore surface by a specific interaction. (b) Type of Figure 4k,l; the virus pulses were trapped inside from the narrowest point of the pore. (c) Behavior type of Figure 4m−o. The virus particles were captured on the pore surface multiple times and then released from the pore. (d) Translocation type of Figure 4p−y. The viruses were not trapped on the nonspecific pore surface.

changes that stopped temporarily at the bottom (Figure 4a−j), which indicates that the viruses were trapped at the narrow end of the conical pore (the point where the pore cross-sectional area is the smallest, Figure 5a). Consequently, the current stopped when the ion blockade was maximized. As shown in Figure 4k,l, the current changes did not stop at the bottom, which indicates that the virus was not trapped at the narrowest point and instead trapped inside the pore. As a result, the current-stopped area in the pulse shape appeared at slightly higher than bottom (Figure 5b). Moreover, trapping of the virus particles did not always occur only one time. Figure 4m−o shows that the current changes stopped a few times, indicating multiple entrapments of the virus particles on the pore surfaces in the translocation process (Figure 5c). In contrast, current changes did not stop in the translocation processes when viral particles were measured using the 3′-sialyllactose-immobilized pore (Figure 4p−y). The nonspecific interactions of the pore surface showed the extension of the translocation time compared with the bare polyurethane surface (Figure 2i); however, this interaction was not strong enough to trap viral particles on the pore surface.

Note that the pulses in Figure 4 were captured where the interaction is clearly visible. The interaction is stochastic, and

https://doi.org/10.1021/acsami.1c25006
ACS Appl. Mater. Interfaces 2022, 14, 20168−20178

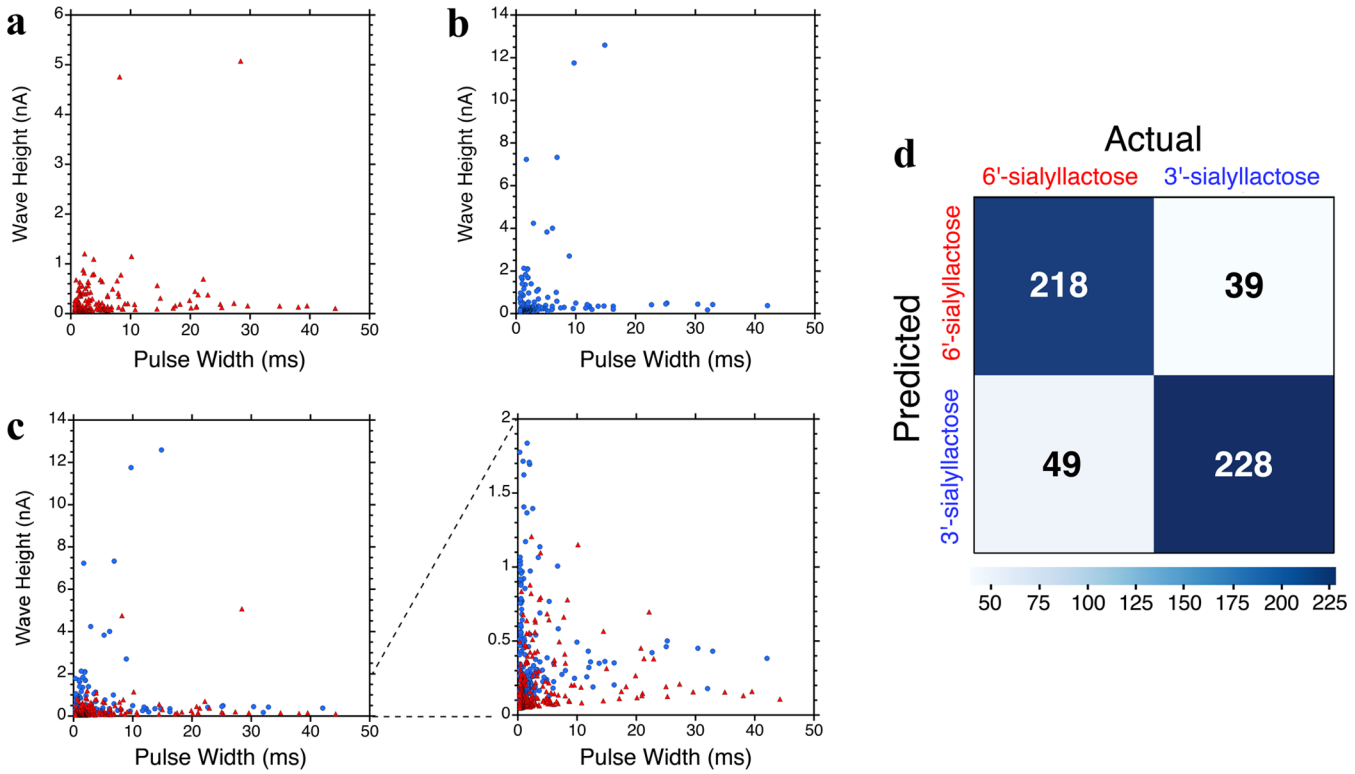

Figure 6. Scatter plots of pulse width (ms) vs height (nA). (a) Red dots describe the pulses generated by the translocations of virus through the 6′-sialyllactose-immobilized pore (specific). (b) Blue dots are generated by the translocation through the 3′-sialyllactose-immobilized pore (nonspecific). (c) Merged data of (a,b). (d) Confusion matrix of the pulse discrimination by the trained machine learning model. Upper left and lower right are the numbers the model successfully classified to true. The accuracy and F-measure values were 0.835 and 0.835, respectively.

there are cases where the interaction is weak or absent. Therefore, there is a limit to classifying these interactions visually, and a more developed evaluation method is needed to solve this problem.

Advanced Evaluation of the Virus Translocation Process. A biosensing technique on RPS is a promising method to selectively detect target particles. Target particles are trapped on the pore surface, which can be monitored by pulse shapes. This translocation process is a stochastic phenomenon in which the translocation time of the particles has a large distribution range. As previously mentioned, the dissociation constant (K_d) between influenza virus and a sialic acid-immobilized surface is 1×10^{-7} M;[63] however, this interaction strength is caused by multivalent bindings. For example, the equilibrium dissociation constant (K_d) range of a lectin−carbohydrate binding is 10^{-2} to 10^{-5} M.[65] Therefore, the binding strength depends on the degree of multivalent bindings. For example, the trapped time of the virus particle in Figure 4j is longer than 10 ms, while the trapped time in Figure 4k is less than 2 ms. As a result, more than 60% of the translocation time distribution histograms overlap between specific and nonspecific binding (Figure 3h), which makes it difficult to use the simple translocation time parameter to divide the specific and nonspecific groups.

Various approaches may be considered to improve the measurement result. One is to increase the binding strength for detection. For example, increasing the density of a ligand on a surface will increase multivalent bindings, reducing the overlapped area between specific and nonspecific bindings. In this method, the risk of pore clogging, one of the most significant problems of the RPS measurement, also increases. Once a clog has occurred, the measurement will stop completely until the clogging problem has been removed. Particle trapping on the pore surface shows a traffic jam of translocations, which is a risk to inducing a pore clog. In our experiment, the pore was clogged immediately at the viral particle measurement when the 6′-siallylactose immobilization efficacy was increased. As a result, this approach is not suitable.

The other approach is detailing the time traces of individual events measured by qNano via AI. The measured pulses have the information for classifying specific and nonspecific binding during the translocation process. However, analysis software for qNano (Control Suite) can only export a limited number of parameters such as the translocation time and pulse wave height. Therefore, a machine learning technique was used instead of the default software. AI technology, including machine learning, is an emerging method to classify measured particles. For example, an ultrathin nanopore (low aspect ratio nanopore) with machine learning can distinguish measured viral particles[12−14] because the ultrathin nanopore can measure the cross-sectional information of particles by blocking the current changes.[23,66] In this method, the feature values extracted from the obtained pulses then apply to the classification model (i.e., support vector machine, random forest, rotation forest, or neural network). Finally, optimization of the decision boundary was performed for the identification of particle species.

In the case of nanopores for qNano, the thickness of the nanopore membrane is several tens of micrometers,[54] which is much larger than the nanoparticles (high aspect ratio pore). Although not as accurate as low aspect ratio pores, high aspect ratio pores can also be used to determine particle shape

https://doi.org/10.1021/acsami.1c25006
ACS Appl. Mater. Interfaces 2022, 14, 20168−20178

information and other information from the pulse shape.[24,25] Therefore, it can be effectively used for machine learning even at high aspect ratios. In addition, an extremely thick pore membrane has a greater chance to interact with measured particles when a biosensing surface is fabricated on a pore surface. Nearly all of the particles are affected by the pore surface according to the translocation time of the viral particles (Figure 2i,j). Therefore, machine learning was applied to pulses measured from 6′-siallylactose- and 3′-siallylactose-immobilized surfaces to investigate the usability of this approach.

In this evaluation, 267 pulses were obtained as feature value sets from the influenza virus translocations through the 6′-sialyllactose-immobilized pore for the machine learning training. 334 pulses obtained as feature value sets from the 3′-sialyllactose pore translocation were used for the training as well. Many of the pulses identified by the pulse extraction procedure for the qNano include fluctuations in the current value and noise so that it is difficult to visually judge whether they are pulses or not. For machine learning, the baseline estimation was performed using a Kalman filter to remove the noise and extract the pulses from current data. Because machine learning identifies pulses by their waveforms, the criteria for being processed as a pulse is stricter than for the qNano. As a result, the number of pulses used for machine learning is fewer than for the qNano. The average baseline duration time for machine learning was 5.08 ms, which differs from that for qNano of 7.02 ms. The result shows that the pulse selection made by the machine learning is systematically different from qNano.

The pulses were then used for machine learning. This algorithm has been implemented in the Aipore-One, an AI particle analysis software, as previously reported.[67] The feature value sets (i.e., measured pulses) were randomly selected so that the number of feature value sets of the two trainings were the same to create a fair discriminator. A series of machine learning algorithms based on the shape of waveforms have been previously described.[67] Figure 6 shows the plots of the height and width of the pulses used for the training. Distributions of the 6′-sialyllactose (Figure 6a) and 3′-sialyllactose (Figure 6b) plots overlapped extensively, and it was difficult to draw a boundary to divide the two groups (Figure 6c). Note that the pulse widths (baseline duration) estimated by the qNano and those estimated for machine learning were not the same because of the different baseline estimation methods.

Because the obtained feature space is multidimensional, it is difficult to visually identify the classification boundaries as shown in the scatter plot in Figure 6c. Therefore, the confusion matrix of the cross validation is shown in Figure 6d as an evaluation of machine learning. The accuracy of the discrimination, the number of pulses correctly predicted by the trained model divided by the total pulse number, was 0.835. The F-measure, the harmonic average of the precision and recall, is commonly used to evaluate the accuracy of a model on a dataset, and the result was 0.835. The F-measure is the discrimination accuracy for a single pulse, namely, the confidence interval will be infinitely close to 1 by increasing the number of pulses for identification. Therefore, the result indicates that nearly certain identification can be obtained by several pulses.

Prospects of PD-Based Biosensing on RPS. According to these evaluations, biosensing on RPS is a promising technique to detect the specific interaction. The translocation processes of viral particles change according to the surface type of pores, such as 6′-sialyllactose and 3′-sialyllactose (Figure 3a,b), which can be recorded as pulse shapes. Therefore, the measurement results of the virus particles could clearly distinguish the difference between the two surfaces. The simple and versatile PD-based biosensor surface design worked effectively. This biosensing technique is a fundamentally different mechanism than conventional biosensing systems, which would be a breakthrough of biosensors. For example, a sensing system for monitoring intermolecular interaction such as SPR, QCM, and SAW sensors measures collective adsorptions and dissociations of analytes, while RPS monitors a translocation process of analytes individually, which will work well for trace analysis. However, the obtained translocation processes including specific interaction of these particles are stochastic, and there are cases where the interaction is long and cases where it is very short or absent. Consequently, the translocation time of viral particles varies over a very wide range depending on the degree of interaction, and the particles cannot be simply classified by the presence or absence of interactions. Therefore, RPS needs to be improved to identify individual particles and details of their interactions such as the kinetic parameter.

A goal of RPS is to identify pathogenic particles for diagnostic purposes. While the results of this study clearly confirmed the existence of virus−pore surface interactions, the stochastic nature of the virus−pore surface interaction makes it difficult to identify particles one by one in the current method. To detect a specific virus among the foreign particles, it is necessary to improve RPS including a design of pores that can generate interactions efficiently. Additionally, there have been attempts to identify this solely through AI particle analysis without any interaction such as biosensors.[13,16,67] If biosensing on a pore surface is incorporated, the identification performance would be further improved by the addition of specific interactions. In most cases, the RPS measures at least a few dozen particles, so even if it is not possible to identify each passing particle individually, it is possible to determine the type of pathogenic particles in a sample. A PD-based biosensing surface may be a versatile technique to support the identification of particle species on RPS.

CONCLUSIONS

In this report, a methodology of biosensing on RPS was investigated. An important process for biosensing on RPS is the preparation of the pore surface. As a versatile surface modification method, a PD-based layer was fabricated on the pore surface, and then sialic acids were immobilized for influenza virus detection. The measured viral particles were trapped on the biosensing surface and the translocation time of the particles increased. According to the measured RPS data, the translocation processes showed different trends for specific and nonspecific surfaces. In our experiment, the difference was evaluated using machine learning; however, any method will work if the difference of the translocation processes can be evaluated. Biosensing on RPS can detect a target via a mechanism different from conventional analytical techniques, which can expand the research area of biosensors.

EXPERIMENTAL SECTION

Materials, Reagents, and Equipment. 3-Hydroxytyramine (dopamine) hydrochloride, AOUT, 6′-sialyllactose (Neu5Acα(2−

https://doi.org/10.1021/acsami.1c25006
ACS Appl. Mater. Interfaces 2022, 14, 20168−20178

6)Galβ(1−4)Glc) sodium salt, and 3′-sialyllactose (Neu5Acα(2−3)Galβ(1−4)Glc) sodium salt were purchased from Tokyo Chemical Industry Co., Ltd., Tokyo, Japan. The particle measurements were performed using a qNano nanoparticle analyzer, NP100 (nanopore, conical hole formed on a polyurethane membrane), and CPC100B (standard polystyrene nanoparticles for calibration, mode size: 110 nm, mean size: 110 nm, raw concentration: 1.0×10^{13} particles/mL) purchased from Izon Science Ltd., Christchurch, New Zealand. Human influenza A virus subtype H1N1 (A/PR/8/34) was grown in embryonated chicken eggs. This growth was carried out in a biosafety level 2 laboratory. The collected virus solutions were detoxified using a 0.05% formaldehyde solution. The characteristics of the virus and the specific interaction between the virus and 6′-sialyllactose were previously reported.[30,58] A NAPiCOS (QCM, Nihon Denpa Kogyo Co., Ltd., Tokyo, Japan) system was used.

Preparation of the Biosensing Surface on the Pores. The preparation of the PD layer on a nanopore was previously reported.[50,51] A pore was soaked in 2 mg/mL dopamine solution [10 mM of Tris-buffer (pH 8.5)] for 15 min in a 25 mL conical tube. This operation was performed on a microplate mixer (shaker) to fill the pore with solution. TRPS can adjust the pore size by applying a stretch; however, the process of surface modification was carried out without the stretch. The pore was washed with deionized (DI) water and then soaked in 1 mM AOUT ethanol solution (15 h, 4 °C) to immobilize AOUT molecules on the PD layer via Michael-type addition.[49] The pore was then washed by ethanol and DI water. The pore was immersed in 0.1 mM 6′-sialyllactose solution (pH 5.3, acetic acid) for 30 min at RT for 6′-sialyllactose immobilization via a condensation reaction between the aminooxyl group and glucose.[57,58] As a control experiment, 3′-sialyllactose-immobilized pore was also prepared using the same method.

QCM Measurements. To estimate the amount of immobilized 6′-sialyllactose indirectly as supplementary data, the same experiment was performed using QCM measurements. The surface immobilization procedure was the same as the case of the pore. The gold sensor chips were exposed in 2 mg/mL dopamine solution [10 mM of Tris-buffer (pH 8.5)] for 15 min. The relative frequency changes were converted to the immobilized amount of the PD layer (Table S1). PD-immobilized QCM sensor chips were soaked in 1 mM AOUT ethanol solution (15 h, 4 °C). These sensor chips were then exposed to 0.1 mM 6′-sialyllactose solution (pH 5.3, acetic acid) for 30 min at RT for 6′-sialyllactose immobilization via a condensation reaction between the aminooxyl group and glucose.[57,58] The relative frequency changes were converted to immobilized amounts of 6′-sialyllactose molecules (Table S2).

Measurement of Human Influenza A Virus Subtype H1N1. A 6′-sialyllactose-immobilized pore was placed on a fluid cell of the qNano particle analyzer, and both sides of the pore were filled with ×0.33 PBS (1/3 PBS). After conduction of the device, the virus was placed on a fluid cell for measurement (2.08×10^8 particles/mL). The applied pressure, stretch, and voltage were 1 kPa, 47.01 mm, and 1.5 V, respectively. These parameters affect the measurement conditions. For example, an applied stretch changes the ionic current by controlling the pore size.[54] The pressure was applied to force the nearly electrically neutral virus particles to pass through. As a control experiment, a 3′-sialyllactose-immobilized pore was used for the virus measurement under the same condition. Virus particle measurements were performed once per pore. The experiment was conducted several times using different pores, including a reproduction experiment. The minimum wave height, baseline duration, and fwhm duration identified as pulses in the particle measurements were 0.01 nA, 0.2 ms, and 0.05 ms, respectively.

Machine Learning Procedure. The pulse extraction procedure was previously reported.[67] The baseline current curve, which is the current without particle translocation, was calculated using the Kalman filter algorithm. The pulses generated by translocation of viruses through a pore were extracted by the baseline. Feature values, which describe the pulse shape, were calculated from each pulse. The feature values calculated from a pulse were called a "feature value set." Many pulses and feature value sets were obtained from a measurement because the samples contained a lot of particles. The details of the definition of the F-measure (F_{meas}) are shown in the Supporting Information.

The machine learning model was trained using 267 pulses of 6′-sialyllactose and 334 pulses of 3′-sialyllactose as feature value sets. Here, training describes the optimization of the parameters in the machine learning model. The extraction procedure of the feature value from the pulse shape is also based on a previous report.[67] The classification model which was implemented in the Aipore-One,[67] an AI particle analysis software provided by Aipore Inc., Tokyo, Japan, was used in this study.

To prevent bias in the results of machine learning, the number of pulses in each group was aligned. Namely, 267 pulses of 3′-sialyllactose were selected randomly for machine learning. A 10-fold cross-validation method was used to evaluate the discriminability of the trained model. Ninety percent of the extracted pulses were randomly selected and used for training, and the remaining 10% of extracted pulses were used for validation for each measurement. The trained model was validated by the remaining 10%, and this validation was repeated 10 times by shifting the feature value sets. The validation result is shown in Figure 6d as a confusion matrix (267 + 267 = 534 events).

■ ASSOCIATED CONTENT

Supporting Information

The Supporting Information is available free of charge at https://pubs.acs.org/doi/10.1021/acsami.1c25006.

Definition of F-measure (F_{meas}), scatter plots of the virus measurements by RPS, reproducibility of translocation time differences by the type of immobilized oligosaccharide, and QCM measurement results (PDF)

■ AUTHOR INFORMATION

Corresponding Author

Yukichi Horiguchi − *Institute of Biomaterials and Bioengineering, Tokyo Medical and Dental University (TMDU), Tokyo 101-0062, Japan*; orcid.org/0000-0002-6748-9643; Email: horiguchi.bsr@tmd.ac.jp

Authors

Norihiko Naono − *Aipore Inc., Tokyo 150-8512, Japan*

Osamu Sakamoto − *Aipore Inc., Tokyo 150-8512, Japan*

Hiroaki Takeuchi − *Department of Molecular Virology, Graduate School of Medical and Dental Sciences, Tokyo Medical and Dental University (TMDU), Tokyo 113-8510, Japan*

Shoji Yamaoka − *Department of Molecular Virology, Graduate School of Medical and Dental Sciences, Tokyo Medical and Dental University (TMDU), Tokyo 113-8510, Japan*

Yuji Miyahara − *Institute of Biomaterials and Bioengineering, Tokyo Medical and Dental University (TMDU), Tokyo 101-0062, Japan*; orcid.org/0000-0003-2703-0958

Complete contact information is available at: https://pubs.acs.org/10.1021/acsami.1c25006

Author Contributions

Y.H. and Y.M. conceived the idea for this project. H.T. and S.Y. performed the preparation of human influenza A virus subtype H1N1 (A/PR/8/34). N.N. and O.S. performed machine learning. Y.H. performed all other experiments. Y.H. wrote this manuscript, and all authors have approved the manuscript and agree with submission.

Funding

This work was supported by JSPS KAKENHI (grant number JP19K05225), the Asahi Glass Foundation, and the Impulsing Paradigm Change through Disruptive Technologies (ImPACT) Miyata Program on the "Ultra high-speed multiplexed sensing system beyond evolution for the detection of extremely small amounts of substances" from Japan Science and Technology (JST) Agency.

Notes

The authors declare no competing financial interest.

■ ACKNOWLEDGMENTS

We thank Ashleigh Cooper, PhD, from Edanz (https://jp.edanz.com/ac) for editing a draft of this manuscript.

■ REFERENCES

(1) DeBlois, R. W.; Bean, C. P. Counting and Sizing of Submicron Particles by the Resistive Pulse Technique. *Rev. Sci. Instrum.* **1970**, *41*, 909−916.
(2) Weatherall, E.; Willmott, G. R. Applications of Tunable Resistive Pulse Sensing. *Analyst* **2015**, *140*, 3318−3334.
(3) Postma, H. W. C. Rapid Sequencing of Individual DNA Molecules in Graphene Nanogaps. *Nano Lett.* **2010**, *10*, 420−425.
(4) Merchant, C. A.; Healy, K.; Wanunu, M.; Ray, V.; Peterman, N.; Bartel, J.; Fischbein, M. D.; Venta, K.; Luo, Z.; Johnson, A. T. C.; Drndić, M. DNA Translocation through Graphene Nanopores. *Nano Lett.* **2010**, *10*, 2915−2921.
(5) Yusko, E. C.; Johnson, J. M.; Majd, S.; Prangkio, P.; Rollings, R. C.; Li, J.; Yang, J.; Mayer, M. Controlling Protein Translocation through Nanopores with Bio-Inspired Fluid Walls. *Nat. Nanotechnol.* **2011**, *6*, 253−260.
(6) Wharton, J. E.; Jin, P.; Sexton, L. T.; Horne, L. P.; Sherrill, S. A.; Mino, W. K.; Martin, C. R. A Method for Reproducibly Preparing Synthetic Nanopores for Resistive-Pulse Biosensors. *Small* **2007**, *3*, 1424−1430.
(7) Takakura, T.; Yanagi, I.; Goto, Y.; Ishige, Y.; Kohara, Y. Single-Molecule Detection of Proteins with Antigen-Antibody Interaction Using Resistive-Pulse Sensing of Submicron Latex Particles. *Appl. Phys. Lett.* **2016**, *108*, 123701.
(8) Healey, M. J.; Sivakumaran, M.; Platt, M. Rapid Quantification of Prion Proteins Using Resistive Pulse Sensing. *Analyst* **2020**, *145*, 2595−2601.
(9) Ali, M.; Ramirez, P.; Tahir, M. N.; Mafe, S.; Siwy, Z.; Neumann, R.; Tremel, W.; Ensinger, W. Biomolecular Conjugation inside Synthetic Polymer Nanopores Viaglycoprotein−Lectin Interactions. *Nanoscale* **2011**, *3*, 1894−1903.
(10) Uram, J. D.; Ke, K.; Hunt, A. J.; Mayer, M. Submicrometer Pore-Based Characterization and Quantification of Antibody−Virus Interactions. *Small* **2006**, *2*, 967−972.
(11) Vogel, R.; Willmott, G.; Kozak, D.; Roberts, G. S.; Anderson, W.; Groenewegen, L.; Glossop, B.; Barnett, A.; Turner, A.; Trau, M. Quantitative Sizing of Nano/Microparticles with a Tunable Elastomeric Pore Sensor. *Anal. Chem.* **2011**, *83*, 3499−3506.
(12) Arima, A.; Harlisa, I. H.; Yoshida, T.; Tsutsui, M.; Tanaka, M.; Yokota, K.; Tonomura, W.; Yasuda, J.; Taniguchi, M.; Washio, T.; Okochi, M.; Kawai, T. Identifying Single Viruses Using Biorecognition Solid-State Nanopores. *J. Am. Chem. Soc.* **2018**, *140*, 16834−16841.
(13) Arima, A.; Tsutsui, M.; Harlisa, I. H.; Yoshida, T.; Tanaka, M.; Yokota, K.; Tonomura, W.; Taniguchi, M.; Okochi, M.; Washio, T.; Kawai, T. Selective Detections of Single-Viruses Using Solid-State Nanopores. *Sci. Rep.* **2018**, *8*, 16305.
(14) Arima, A.; Tsutsui, M.; Yoshida, T.; Tatematsu, K.; Yamazaki, T.; Yokota, K.; Kuroda, S. i.; Washio, T.; Baba, Y.; Kawai, T. Digital Pathology Platform for Respiratory Tract Infection Diagnosis Via Multiplex Single-Particle Detections. *ACS Sens.* **2020**, *5*, 3398−3403.
(15) Yu, A. C. S.; Loo, J. F. C.; Yu, S.; Kong, S. K.; Chan, T.-F. Monitoring Bacterial Growth Using Tunable Resistive Pulse Sensing with a Pore-Based Technique. *Appl. Microbiol. Biotechnol.* **2014**, *98*, 855−862.
(16) Tsutsui, M.; Yoshida, T.; Yokota, K.; Yasaki, H.; Yasui, T.; Arima, A.; Tonomura, W.; Nagashima, K.; Yanagida, T.; Kaji, N.; Taniguchi, M.; Washio, T.; Baba, Y.; Kawai, T. Discriminating Single-Bacterial Shape Using Low-Aspect-Ratio Pores. *Sci. Rep.* **2017**, *7*, 17371.
(17) Böing, A. N.; van der Pol, E.; Grootemaat, A. E.; Coumans, F. A. W.; Sturk, A.; Nieuwland, R. Single-Step Isolation of Extracellular Vesicles by Size-Exclusion Chromatography. *J. Extracell. Vesicles* **2014**, *3*, 23430.
(18) Nizamudeen, Z.; Markus, R.; Lodge, R.; Parmenter, C.; Platt, M.; Chakrabarti, L.; Sottile, V. Rapid and Accurate Analysis of Stem Cell-Derived Extracellular Vesicles with Super Resolution Microscopy and Live Imaging. *Biochim. Biophys. Acta, Mol. Cell Res.* **2018**, *1865*, 1891−1900.
(19) Kei, K.; Masashi, K.; Nami, H.; Takanori, A.; Nobuyoshi, K.; Takahiro, O.; Takanori, I. Electrokinetic Evaluation of Individual Exosomes by on-Chip Microcapillary Electrophoresis with Laser Dark-Field Microscopy. *Jpn. J. Appl. Phys.* **2013**, *52*, 06GK10.
(20) Zhang, H.; Freitas, D.; Kim, H. S.; Fabijanic, K.; Li, Z.; Chen, H.; Mark, M. T.; Molina, H.; Martin, A. B.; Bojmar, L.; Fang, J.; Rampersaud, S.; Hoshino, A.; Matei, I.; Kenific, C. M.; Nakajima, M.; Mutvei, A. P.; Sansone, P.; Buehring, W.; Wang, H.; Jimenez, J. P.; Cohen-Gould, L.; Paknejad, N.; Brendel, M.; Manova-Todorova, K.; Magalhães, A.; Ferreira, J. A.; Osório, H.; Silva, A. M.; Massey, A.; Cubillos-Ruiz, J. R.; Galletti, G.; Giannakakou, P.; Cuervo, A. M.; Blenis, J.; Schwartz, R.; Brady, M. S.; Peinado, H.; Bromberg, J.; Matsui, H.; Reis, C. A.; Lyden, D. Identification of Distinct Nanoparticles and Subsets of Extracellular Vesicles by Asymmetric Flow Field-Flow Fractionation. *Nat. Cell Biol.* **2018**, *20*, 332−343.
(21) Anderson, W.; Kozak, D.; Coleman, V. A.; Jämting, Å. K.; Trau, M. A Comparative Study of Submicron Particle Sizing Platforms: Accuracy, Precision and Resolution Analysis of Polydisperse Particle Size Distributions. *J. Colloid Interface Sci.* **2013**, *405*, 322−330.
(22) Akpinar, F.; Yin, J. Characterization of Vesicular Stomatitis Virus Populations by Tunable Resistive Pulse Sensing. *J. Virol. Methods* **2015**, *218*, 71−76.
(23) Ryuzaki, S.; Makusu, T.; Yuhui, H.; Kazumichi, Y.; Akihide, A.; Takanori, M.; Masateru, T.; Tomoji, K. Rapid Structural Analysis of Nanomaterials in Aqueous Solutions. *Nanotechnology* **2017**, *28*, 155501.
(24) Qiu, Y.; Hinkle, P.; Yang, C.; Bakker, H. E.; Schiel, M.; Wang, H.; Melnikov, D.; Gracheva, M.; Toimil-Molares, M. E.; Imhof, A.; Siwy, Z. S. Pores with Longitudinal Irregularities Distinguish Objects by Shape. *ACS Nano* **2015**, *9*, 4390−4397.
(25) Maugi, R.; Hauer, P.; Bowen, J.; Ashman, E.; Hunsicker, E.; Platt, M. A Methodology for Characterising Nanoparticle Size and Shape Using Nanopores. *Nanoscale* **2020**, *12*, 262−270.
(26) Kozak, D.; Anderson, W.; Vogel, R.; Chen, S.; Antaw, F.; Trau, M. Simultaneous Size and Z-Potential Measurements of Individual Nanoparticles in Dispersion Using Size-Tunable Pore Sensors. *ACS Nano* **2012**, *6*, 6990−6997.
(27) Horiguchi, Y.; Miyachi, S.; Nagasaki, Y. High-Performance Surface Acoustic Wave Immunosensing System on a PEG/Aptamer Hybridized Surface. *Langmuir* **2013**, *29*, 7369−7376.
(28) Horiguchi, Y.; Nakayama, N.; Kanayama, N.; Nagasaki, Y. Sulfobetaine-Terminated Peg Improves the Qualities of an Immunosensing Surface. *Biomater. Sci.* **2014**, *2*, 819−826.
(29) Freedman, K. J.; Bastian, A. R.; Chaiken, I.; Kim, M. J. Solid-State Nanopore Detection of Protein Complexes: Applications in Healthcare and Protein Kinetics. *Small* **2013**, *9*, 750−759.
(30) Horiguchi, Y.; Goda, T.; Matsumoto, A.; Takeuchi, H.; Yamaoka, S.; Miyahara, Y. Gold Nanoparticles with Ligand/Zwitterion Hybrid Layer for Individual Counting of Influenza a H1n1 Subtype Using Resistive Pulse Sensing. *Langmuir* **2019**, *35*, 1798−1806.

(31) Ang, Y. S.; Yung, L.-Y. L. Rapid and Label-Free Single-Nucleotide Discrimination Via an Integrative Nanoparticle−Nanopore Approach. *ACS Nano* **2012**, *6*, 8815−8823.
(32) Mayne, L.; Lin, C.-Y.; Christie, S. D. R.; Siwy, Z. S.; Platt, M. The Design and Characterization of Multifunctional Aptamer Nanopore Sensors. *ACS Nano* **2018**, *12*, 4844−4852.
(33) Heaton, I.; Platt, M. Peptide Nanocarriers for Detection of Heavy Metal Ions Using Resistive Pulse Sensing. *Anal. Chem.* **2019**, *91*, 11291−11296.
(34) Gyurcsányi, R. E. Chemically-Modified Nanopores for Sensing. *Trends Anal. Chem.* **2008**, *27*, 627−639.
(35) Pérez-Mitta, G.; Toimil-Molares, M. E.; Trautmann, C.; Marmisollé, W. A.; Azzaroni, O. Molecular Design of Solid-State Nanopores: Fundamental Concepts and Applications. *Adv. Mater.* **2019**, *31*, 1901483.
(36) Ding, D.; Gao, P.; Ma, Q.; Wang, D.; Xia, F. Biomolecule-Functionalized Solid-State Ion Nanochannels/Nanopores: Features and Techniques. *Small* **2019**, *15*, 1804878.
(37) Wei, R.; Gatterdam, V.; Wieneke, R.; Tampé, R.; Rant, U. Stochastic Sensing of Proteins with Receptor-Modified Solid-State Nanopores. *Nat. Nanotechnol.* **2012**, *7*, 257−263.
(38) Ren, R.; Zhang, Y.; Nadappuram, B. P.; Akpinar, B.; Klenerman, D.; Ivanov, A. P.; Edel, J. B.; Korchev, Y. Nanopore Extended Field-Effect Transistor for Selective Single-Molecule Biosensing. *Nat. Commun.* **2017**, *8*, 586.
(39) Siwy, Z. S. Ion-Current Rectification in Nanopores and Nanotubes with Broken Symmetry. *Adv. Funct. Mater.* **2006**, *16*, 735−746.
(40) Zhang, L.-X.; Cao, X.-H.; Zheng, Y.-B.; Li, Y.-Q. Covalent Modification of Single Glass Conical Nanopore Channel with 6-Carboxymethyl-Chitosan for Ph Modulated Ion Current Rectification. *Electrochem. Commun.* **2010**, *12*, 1249−1252.
(41) Blundell, E. L. C. J.; Mayne, L. J.; Lickorish, M.; Christie, S. D. R.; Platt, M. Protein Detection Using Tunable Pores: Resistive Pulses and Current Rectification. *Faraday Discuss.* **2016**, *193*, 487−505.
(42) Zhu, Z.; Wang, D.; Tian, Y.; Jiang, L. Ion/Molecule Transportation in Nanopores and Nanochannels: From Critical Principles to Diverse Functions. *J. Am. Chem. Soc.* **2019**, *141*, 8658−8669.
(43) Pérez-Mitta, G.; Albesa, A. G.; Trautmann, C.; Toimil-Molares, M. E.; Azzaroni, O. Bioinspired Integrated Nanosystems Based on Solid-State Nanopores: "Iontronic" Transduction of Biological, Chemical and Physical Stimuli. *Chem. Sci.* **2017**, *8*, 890−913.
(44) Srinivas, A. R. G.; Hilali, R.; Damavandi, M.; Malmstrom, J.; Barker, D.; Weatherall, E.; Willmott, G.; Travas-Sejdic, J. Polymer Brush Functionalization of Polyurethane Tunable Nanopores for Resistive Pulse Sensing. *ACS Appl. Polym. Mater.* **2021**, *3*, 279−289.
(45) Xie, Y.; Xue, J.; Wang, L.; Wang, X.; Jin, K.; Chen, L.; Wang, Y. Surface Modification of Single Track-Etched Nanopores with Surfactant Ctab. *Langmuir* **2009**, *25*, 8870−8874.
(46) Barsbay, M.; Güven, O. Grafting in Confined Spaces: Functionalization of Nanochannels of Track-Etched Membranes. *Radiat. Phys. Chem.* **2014**, *105*, 26−30.
(47) Pan, K.; Ren, R.; Liang, B.; Li, L.; Li, H.; Cao, B. Synthesis of Ph-Responsive Polyethylene Terephthalate Track-Etched Membranes by Grafting Hydroxyethyl-Methacrylate Using Atom-Transfer Radical Polymerization Method. *J. Appl. Polym. Sci.* **2014**, *131*, 40912.
(48) Lee, H.; Dellatore, S. M.; Miller, W. M.; Messersmith, P. B. Mussel-Inspired Surface Chemistry for Multifunctional Coatings. *Science* **2007**, *318*, 426−430.
(49) Wu, J.; Zhang, L.; Wang, Y.; Long, Y.; Gao, H.; Zhang, X.; Zhao, N.; Cai, Y.; Xu, J. Mussel-Inspired Chemistry for Robust and Surface-Modifiable Multilayer Films. *Langmuir* **2011**, *27*, 13684−13691.
(50) Horiguchi, Y.; Goda, T.; Miyahara, Y. Simple Functionalization Method for Single Conical Pores with a Polydopamine Layer. *Appl. Phys. Express* **2018**, *11*, 047001.
(51) Horiguchi, Y.; Miyahara, Y. Surface Modification to Suppress Small Pore Clogging in Resistive Pulse Sensing. *Appl. Phys. Express* **2020**, *13*, 115002.
(52) Sowerby, S. J.; Broom, M. F.; Petersen, G. B. Dynamically Resizable Nanometre-Scale Apertures for Molecular Sensing. *Sens. Actuators, B* **2007**, *123*, 325−330.
(53) Kozak, D.; Anderson, W.; Vogel, R.; Trau, M. Advances in Resistive Pulse Sensors: Devices Bridging the Void between Molecular and Microscopic Detection. *Nano Today* **2011**, *6*, 531−545.
(54) Kozak, D.; Anderson, W.; Grevett, M.; Trau, M. Modeling Elastic Pore Sensors for Quantitative Single Particle Sizing. *J. Phys. Chem. C* **2012**, *116*, 8554−8561.
(55) Stanley, W. M. The Size of Influenza Virus. *J. Exp. Med.* **1944**, *79*, 267−283.
(56) Wiley, D. C.; Skehel, J. J. The Structure and Function of the Hemagglutinin Membrane Glycoprotein of Influenza Virus. *Annu. Rev. Biochem.* **1987**, *56*, 365−394.
(57) Hideshima, S.; Hinou, H.; Ebihara, D.; Sato, R.; Kuroiwa, S.; Nakanishi, T.; Nishimura, S.-I.; Osaka, T. Attomolar Detection of Influenza a Virus Hemagglutinin Human H1 and Avian H5 Using Glycan-Blotted Field Effect Transistor Biosensor. *Anal. Chem.* **2013**, *85*, 5641−5644.
(58) Horiguchi, Y.; Goda, T.; Matsumoto, A.; Takeuchi, H.; Yamaoka, S.; Miyahara, Y. Direct and Label-Free Influenza Virus Detection Based on Multisite Binding to Sialic Acid Receptors. *Biosens. Bioelectron.* **2017**, *92*, 234−240.
(59) Willmott, G. R.; Vogel, R.; Yu, S. S. C.; Groenewegen, L. G.; Roberts, G. S.; Kozak, D.; Anderson, W.; Trau, M. Use of Tunable Nanopore Blockade Rates to Investigate Colloidal Dispersions. *J. Phys.: Condens. Matter* **2010**, *22*, 454116.
(60) Willmott, G. R.; Chaturvedi, R.; Cummins, S. J. W.; Groenewegen, L. G. Actuation of Tunable Elastomeric Pores: Resistance Measurements and Finite Element Modelling. *Exp. Mech.* **2014**, *54*, 153−163.
(61) Tsutsui, M.; Hongo, S.; He, Y.; Taniguchi, M.; Gemma, N.; Kawai, T. Single-Nanoparticle Detection Using a Low-Aspect-Ratio Pore. *ACS Nano* **2012**, *6*, 3499−3505.
(62) Platt, M.; Willmott, G. R.; Lee, G. U. Resistive Pulse Sensing of Analyte-Induced Multicomponent Rod Aggregation Using Tunable Pores. *Small* **2012**, *8*, 2436−2444.
(63) Takemoto, D. K.; Skehel, J. J.; Wiley, D. C. A Surface Plasmon Resonance Assay for the Binding of Influenza Virus Hemagglutinin to Its Sialic Acid Receptor. *Virology* **1996**, *217*, 452−458.
(64) Narayanan, S. Sialic Acid as a Tumor Marker. *Ann. Clin. Lab. Sci.* **1994**, *24*, 376−384.
(65) Lis, H.; Sharon, N. Lectins: Carbohydrate-Specific Proteins That Mediate Cellular Recognition. *Chem. Rev.* **1998**, *98*, 637−674.
(66) Goyal, G.; Mulero, R.; Ali, J.; Darvish, A.; Kim, M. J. Low Aspect Ratio Micropores for Single-Particle and Single-Cell Analysis. *Electrophoresis* **2015**, *36*, 1164−1171.
(67) Taniguchi, M.; Minami, S.; Ono, C.; Hamajima, R.; Morimura, A.; Hamaguchi, S.; Akeda, Y.; Kanai, Y.; Kobayashi, T.; Kamitani, W.; Terada, Y.; Suzuki, K.; Hatori, N.; Yamagishi, Y.; Washizu, N.; Takei, H.; Sakamoto, O.; Naono, N.; Tatematsu, K.; Washio, T.; Matsuura, Y.; Tomono, K. Combining Machine Learning and Nanopore Construction Creates an Artificial Intelligence Nanopore for Coronavirus Detection. *Nat. Commun.* **2021**, *12*, 3726.

https://doi.org/10.1021/acsami.1c25006
ACS Appl. Mater. Interfaces 2022, 14, 20168−20178